Quantitative mass spectrometry reveals a role for the GTPase Rho1p in actin organization on the peroxisome membrane

Marcello Marelli,[1] Jennifer J. Smith,[1] Sunhee Jung,[1] Eugene Yi,[1] Alexey I. Nesvizhskii,[1] Rowan H. Christmas,[1] Ramsey A. Saleem,[1] Yuen Yi C. Tam,[2] Andrei Fagarasanu,[2] David R. Goodlett,[1] Ruedi Aebersold,[1] Richard A. Rachubinski,[2] and John D. Aitchison[1,2]

[1]Institute for Systems Biology, Seattle, WA 98103
[2]Department of Cell Biology, University of Alberta, Edmonton, Alberta T6G 2H7, Canada

We have combined classical subcellular fractionation with large-scale quantitative mass spectrometry to identify proteins that enrich specifically with peroxisomes of *Saccharomyces cerevisiae*. In two complementary experiments, isotope-coded affinity tags and tandem mass spectrometry were used to quantify the relative enrichment of proteins during the purification of peroxisomes. Mathematical modeling of the data from 306 quantified proteins led to a prioritized list of 70 candidates whose enrichment scores indicated a high likelihood of them being peroxisomal. Among these proteins, eight novel peroxisome-associated proteins were identified. The top novel peroxisomal candidate was the small GTPase Rho1p. Although Rho1p has been shown to be tethered to membranes of the secretory pathway, we show that it is specifically recruited to peroxisomes upon their induction in a process dependent on its interaction with the peroxisome membrane protein Pex25p. Rho1p regulates the assembly state of actin on the peroxisome membrane, thereby controlling peroxisome membrane dynamics and biogenesis.

Introduction

Although the complete sequence of a genome provides a blueprint for the protein inventory of an organism, understanding the dynamic and responsive organization of a proteome remains a major challenge. Within eukaryotic cells, subcellular organelles are the most obvious level of organization, constituting assemblies of localized proteins that impart efficiency and control over the biochemical functions performed by the proteome. Recent advances that have increased the sensitivity and throughput of mass spectrometry (MS) have made possible the identification of proteins in samples of complexity on the order of organelles. However, the use of MS to comprehensively define organellar protein content is still a formidable undertaking. The polydispersity within organelle classes resulting from biological diversity and the limited resolving power of subfractionation techniques contribute to the notorious problem of organelle contamination by proteins from other cellular compartments. Moreover, the levels of different proteins in an organelle fraction can vary over several orders of magnitude, resulting in highly represented proteins, or even contaminants, dominating the mass spectrometric analysis.

The issue of sample complexity has been addressed at both the prefractionation and instrumentation levels (for review see Aebersold and Mann, 2003). Likewise, various biochemical methods, including serial purification, immunoisolation, and free flow electrophoresis, have been applied to reduce contaminants (for review see Brunet et al., 2003). Although these methods improve sample purity, they remain unable to discriminate between bona fide organelle constituents and residual contaminants.

The problem of contaminants in isolated organelles is not new to the postgenomic era. Classically, de Duve (1992) defined true constituents of a subcellular fraction not as the proteins present in the fraction but rather as the proteins that specifically enrich in that fraction relative to other fractions, a designation that requires knowledge of relative protein abundances. The application of these principles of fractionation analysis to high-throughput proteomics can, in effect, address the issue of contaminating proteins. However, traditional MS is not well

The online version of this article includes supplemental material.

Correspondence to John D. Aitchison: jaitchison@systemsbiology.org

Abbreviations used in this paper: AP, affinity-purified peroxisomal membrane; DsRed, *Discosoma sp.* red fluorescent protein; ICAT, isotope-coded affinity tag; MS, mass spectrometry; μLC/ESI-MS/MS, microcapillary liquid chromatography/electrospray ionization tandem MS; PTS, peroxisomal targeting signal; RFP, monomeric DsRed; SGD, Saccharomyces Genome Database.

The Journal of Cell Biology, Vol. 167, No. 6, December 20, 2004 1099–1112
http://www.jcb.org/cgi/doi/10.1083/jcb.200404119

Supplemental Material can be found at:
http://www.jcb.org/cgi/content/full/jcb.200404119/DC1

suited to this task because the chemical and physical characteristics of a molecule affect many aspects of its ionization and detection, rendering MS inherently poorly quantitative. To overcome this limitation, quantitative proteomic approaches have been developed and successfully applied to the proteomic analyses of complex biological samples (for review see Aebersold and Mann, 2003). One such method is based on the use of isotope-coded affinity tags (ICAT). In this method, peptide pairs in two fractions are discriminated by labeling them with chemically identical, but isotopically different, tags (Gygi et al., 1999). The two fractions can be mixed and analyzed simultaneously to eliminate variability, and the relative abundances of peptides can be determined by their relative signal intensities. Here, we combine high-throughput quantitative MS with classical cell fractionation to identify proteins that specifically enrich with isolated peroxisomes of the yeast *Saccharomyces cerevisiae*.

Peroxisomes perform a variety of regulated metabolic roles including fatty acid metabolism, cholesterol and hormone biosynthesis, and nerve myelination. Remarkably, the size, number, and content of peroxisomes are controlled and modulated in response to extracellular cues. This control of the peroxisome population is most dramatic in yeast, where fatty acid metabolism requires peroxisomes (for review see Veenhuis et al., 2003), but peroxisomes are also induced in metazoan cells in response to fats, hypolipidemic agents, and nongenotoxic carcinogens and to the normal physiological processes of organismal development and cellular differentiation (for review see Weller et al., 2003). Peroxisomes are so dynamic and diverse that today, almost forty years after their initial characterization (Baudhuin et al., 1965), the details of their biochemistry and fundamental aspects of their biogenesis are still unfolding.

Although studies in a variety of organisms have led to the identification of more than thirty well conserved peroxins (proteins involved in peroxisome biogenesis and maintenance), the mechanism of protein translocation across the peroxisomal membrane, the origin of peroxisomes, and the pathways peroxisomes follow to develop and mature remain controversial. For example, studies of peroxisome inheritance in yeast, together with morphological observations in mammalian cells, suggest that peroxisomes develop from preexisting peroxisomes, but compelling evidence has also accumulated supporting the de novo generation of peroxisomes from the endomembrane system/ER of cells (for reviews see Tabak et al., 2003; Veenhuis et al., 2003). Nevertheless, regardless of the origin of peroxisomes, most current models propose that peroxisome maturation involves a multistep assembly process consistent with observations of heterogeneous populations of peroxisomes that differ in size, buoyant density, protein composition, and import capacity (for review see Titorenko and Rachubinski, 2001).

Our limited picture of peroxisome biology and biochemistry suggests that not all peroxisomal proteins have been identified. Some components may remain elusive because of functional redundancy (genetic buffering) or because they have additional functions related to other organelles or cellular processes that are difficult to distinguish from their peroxisome-related functions. Recently, genetic approaches have been complemented with large-scale in silico, proteomic, and transcriptome profiling analyses (for review see Hiltunen et al., 2003) that have not only led to the identification of novel peroxisomal proteins but have also provided large-scale data sets that are essential for building and predicting the behavior of the molecular networks underlying peroxisome assembly and function.

We have combined subcellular fractionation and immunoisolation with large-scale quantitative MS to comprehensively identify proteins that specifically enrich with fractions of peroxisomes purified from *S. cerevisiae*. We first applied microcapillary liquid chromatography/electrospray ionization tandem MS (μLC/ESI-MS/MS) to identify peptides from a purified peroxisomal fraction to generate a list of putative peroxisomal proteins. As the data from this analysis suggested the inclusion of many potential contaminants or proteins shared with other organelles among the true peroxisomal proteins, they were complemented by data from a second approach in which we used quantitative ICAT-based μLC/ESI-MS/MS combined with a novel scoring algorithm to identify proteins that specifically coenrich with the peroxisomal fraction. Several proteins not previously shown to localize with peroxisomes were found to associate with, or function in, diverse aspects of peroxisome biology.

Results

Our objectives were twofold: to improve the application of MS to subcellular localization analysis by discriminating, up-front, proteins that are bona fide components of an organelle from contaminants, and to apply this approach to yeast peroxisomes in an effort to more fully understand the biology of this organelle.

Identification of peroxisomal proteins by quantitative tandem MS

We previously reported the use of automated μLC/ESI-MS/MS using gas-phase fractionation to identify proteins in *S. cerevisiae* peroxisomes (Yi et al., 2002). This approach resulted in the identification of 46 of the 53 known peroxisomal proteins (87% coverage) and included 18 of the known 23 peroxins of *S. cerevisiae*, as annotated by the Saccharomyces Genome Database (SGD; see Tables S1 and S2 for all MS-derived data and protein listings, available at http://www.jcb.org/cgi/content/full/jcb.200404119/DC1). Although the application of gas-phase fractionation resulted in high sample coverage, ~240 different proteins were identified by this analysis, many of which were likely contaminants from other cellular compartments. Indeed, over 54% (130) of these proteins were annotated in SGD as components of other compartments, highlighting the difficulty of attributing protein subcellular location based solely on the comprehensive inventorying of proteins from subcellular fractions.

To discriminate peroxisomal proteins from those that contaminate peroxisome fractions, we combined the principles of classic subcellular fractionation with quantitative MS across different peroxisome purification schemes. In each case, ICAT-

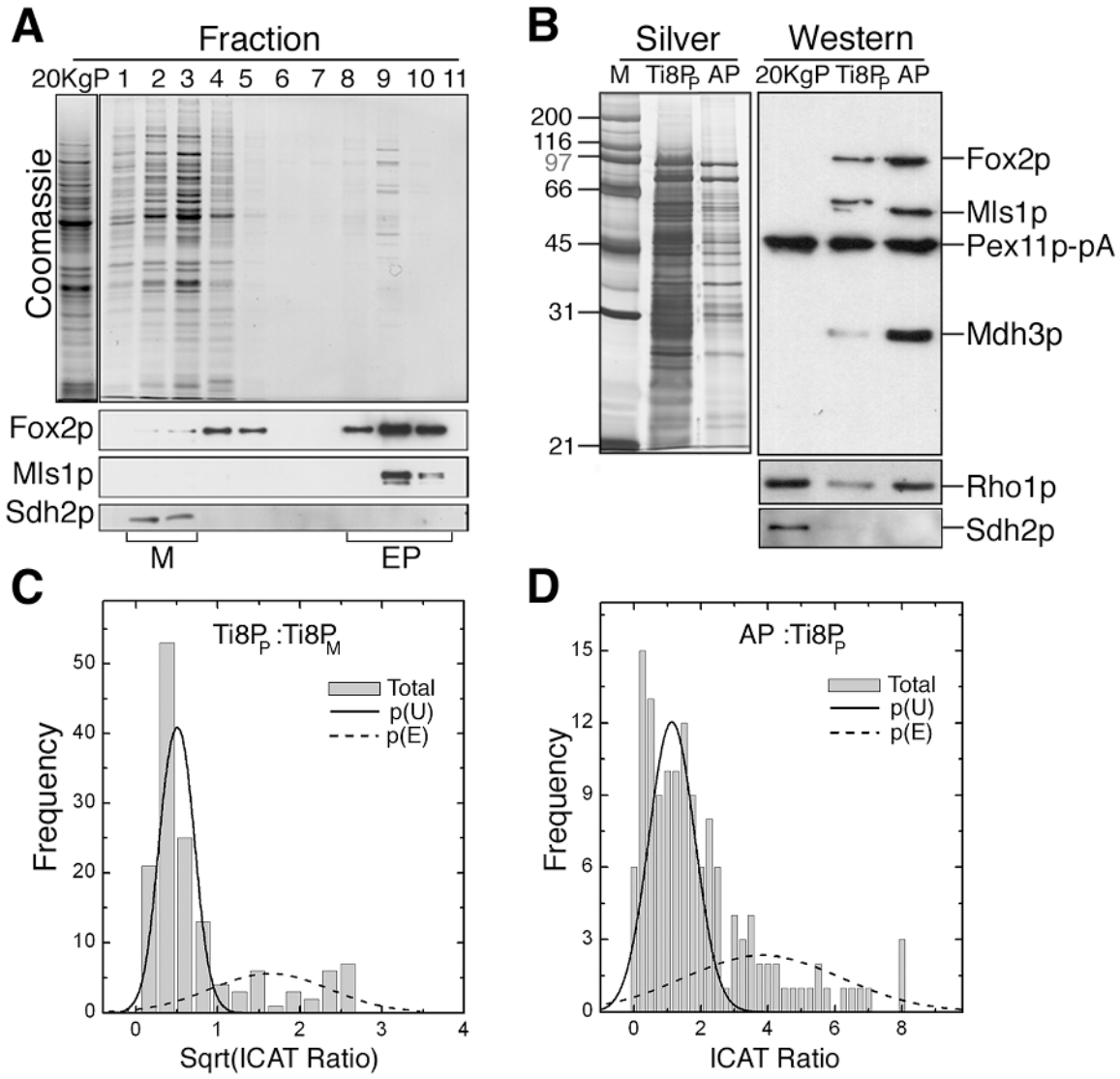

Figure 1. **Sample preparation and analysis.** (A) An organellar 20KgP fraction was subjected to isopycnic density gradient centrifugation and analyzed by SDS-PAGE and Coomassie blue staining (top panel). Fractions enriched for peroxisomes (EP) or mitochondria (M) were identified by Western blotting as shown. Equal amounts of protein derived from each of the hypotonically lysed M and EP fractions were combined and analyzed by ICAT MS/MS. (B) Peroxisomal membranes isolated from a yeast strain synthesizing Pex11p-pA were affinity purified (AP) from a fraction enriched for peroxisomal membranes (Ti8P$_P$). Equal cellular equivalents of each were analyzed by SDS-PAGE and silver staining. Equal amounts of protein from the 20KgP, Ti8P$_P$, and AP fractions were analyzed by Western blotting. Ti8P$_P$ and AP fractions were analyzed by ICAT MS/MS. (C and D) Histograms of ICAT ratios (heavy:light) for 192 proteins quantified in ICAT I (C) and 193 proteins quantified in ICAT II (D). The distributions were modeled by two overlapping Gaussian curves using a partially supervised mixture model Expectation-Maximization algorithm. Note that because of the nature of the data in ICAT I (dominance by mitochondrial proteins with low ICAT ratios and relatively few peroxisomal proteins with high ratios), the ICAT ratios in this experiment were transformed to their square root for modeling. For any quantified protein, the probability of being enriched (p(E); dashed line) or not being enriched (p(U); solid line) with peroxisomes was calculated as a function of its ICAT ratio.

based MS was used to compare the relative abundance of identified proteins in an enriched versus a crude or contaminating fraction. Using this approach, it was possible to identify proteins that specifically enriched through the purification, indicating their association with peroxisomes.

Fractions were differentially labeled with isotopically heavy ($^2H_8$ or $^{13}C_9$) or light ($^1H_8$ or $^{12}C_9$) ICAT reagent, which forms a covalent adduct with the side chains of reduced cysteine amino acyl residues and contains a biotin moiety. Samples were mixed and then fractionated by ion exchange and avidin affinity chromatography before automated gas-phase fractionation and μLC/ESI-MS/MS. The relative abundances of ICAT-labeled peptide pairs were calculated and expressed as the ratios of the signal intensities (see online supplemental material, available at http://www.jcb.org/cgi/content/full/jcb.200404119/DC1). This ratio represents the relative enrichment of proteins through the purification.

In the first approach, ICAT I, organelles from oleic acid-grown cells were collected and separated by isopycnic density gradient centrifugation. Intact organelles were collected from both peak peroxisome (Fig. 1 A, fractions 8–10) and peak mitochondrial (Fig. 1 A, fractions 2 and 3) fractions and hypotonically lysed, and the membrane-enriched fractions were collected by centrifugation. The resulting membrane-enriched

fractions derived from peroxisome ($Ti8P_P$) and mitochondrial ($Ti8P_M$) peak fractions were labeled separately with heavy and light ICAT reagent, respectively, and analyzed by MS (see online supplemental material).

In the second approach, ICAT II, a $Ti8P_P$ was isolated from a yeast strain synthesizing a COOH-terminal chimera of the peroxisomal membrane protein Pex11p (Pex11p-pA [protein A from *Staphylococcus aureus*]). The $Ti8P_P$ fraction was subjected to chromatography on an IgG resin to obtain a fraction of affinity-purified peroxisomal membranes (APs; Fig. 1 B). The $Ti8P_P$ and AP fractions were differentially labeled with light and heavy ICAT reagent, respectively, and analyzed as for ICAT I. A preliminary comparison of the $Ti8P_P$ and AP fractions by SDS-PAGE (Fig. 1 B) revealed a significant reduction in the complexity of the fraction and an increase in the relative abundances of several protein bands. Western blot analysis of equal amounts of protein from the $Ti8P_P$ and AP fractions and from a crude organellar pellet (20KgP) fraction showed a specific enrichment for several peroxisomal proteins in the AP fraction (Fig. 1 B).

A plot of ICAT ratios for all proteins quantified by either ICAT I (Fig. 1 C) or ICAT II (Fig. 1 D) showed a normal distribution with a pronounced shoulder extending in the direction of higher ICAT ratios. The position of each protein on the abscissa represents its ICAT ratio and approximates its relative enrichment ($Ti8P_P$ versus $Ti8P_M$ for ICAT I and AP versus $Ti8P_P$ for ICAT II). These ratios are dependent on the limitations of MS, subcellular fractionation, and biochemical fractionation. Therefore, the probability of being enriched in the enriched peroxisomal membrane fraction (P_E) as a function of its ICAT ratio was determined for each protein (see online supplemental material). Essentially, the distribution of ICAT ratios was modeled using Gaussian distributions, and the mixture model was fitted to the data using an expectation-maximization algorithm. The model was adjusted to take advantage of the fact that some of the identified proteins were previously shown to be peroxisomal, but was not adjusted to account for proteins thought to be "contaminants" (with the exception of ribosomal proteins, which were ignored and not included in the analysis). Importantly, as proteins might be localized to multiple organelles, this approach permitted the inclusion of proteins previously localized to other cellular compartments. However, it should be noted that the method presented here is general and can be applied in a completely unsupervised manner when no relevant prior information is available as to the protein constituents of a particular subcellular compartment (unpublished data). The data from two independent ICAT I and ICAT II experiments were combined, and where two P_E scores were obtained for a protein, the scores were averaged (Fig. 2).

In the case of ICAT I, 346 proteins were identified (23 were annotated in SGD as peroxisomal and 134 as mitochondrial). However, when considering only the 57 proteins in this data set with P_E scores >0.65, 18 were annotated in SGD as peroxisomal ($p = 8.09 \times 10^{-25}$) and none as mitochondrial (p is the probability of identifying proteins annotated with a particular term [in this case localization] by chance from the entire yeast proteome; see online supplemental material and data summaries in Tables S1 and S2). These results indicate that P_E scores from ICAT I provided an excellent mechanism to identify mitochondrial contaminants within the peroxisome fraction. ICAT II identified 365 proteins, 38 of which were annotated in SGD as peroxisomal. 98 proteins had P_E scores >0.65, and 28 of these were annotated as peroxisomal (see online supplemental material).

A comparison of the two data sets highlights the advantages of using complementary experimental approaches to identify constituents of the peroxisome proteome. ICAT I was better than ICAT II at distinguishing mitochondrial contaminants from peroxisomal proteins. This is likely because mitochondrial proteins are abundant contaminants of peroxisome fractions and were easily identified in the mitochondrion-enriched $Ti8P_M$ fraction. However, due to the greater protein complexity of the mixture being analyzed, ICAT I was technically limited in its ability to identify many proteins. Thus, mixing mitochondrial and peroxisome fractions had the effect of reducing the overall number of peroxisomal proteins identified. In addition, ICAT I alone was ineffective in detecting proteins localized specifically to the two organelles that were mixed in the experiment (i.e., peroxisomes and mitochondria). In principle, such proteins should be detectable by integrating data from ICAT II.

ICAT II had the advantage of being able to identify more peroxisomal proteins, including seven additional peroxins. This greater depth is likely because the complexity of the sample was not increased beyond that of the peak peroxisome fractions obtained by density gradient centrifugation. However, the dependence on affinity purification to detect proteins associated with peroxisomal membranes meant that proteins that are particularly abundant, or have some affinity for the resin used in purification, could potentially yield artifactually high P_E scores in ICAT II. However, many of these proteins should be uncovered by relatively low P_E scores in ICAT I.

Prioritization of candidates

Candidate proteins were prioritized for further analysis based on the aforementioned principles of selection for peroxisomal proteins. The core list comprises 98 proteins with high P_E scores (>0.65) in ICAT II. The integration of data from ICAT I analysis and subsequent clustering led to three groupings (Fig. 2 B). Group 1 consists of proteins with high ICAT I P_E scores (>0.6), which are, for the most part, known abundant peroxisomal proteins. Of the 25 proteins in this group, 18 are annotated in SGD as peroxisomal ($p = 1.55 \times 10^{-33}$). Notably, this group contains several proteins dually localized to peroxisomes and other organelles (Table S2). In addition, Group 1 contains seven proteins not previously characterized as peroxisomal, including the lipid body protein Faa1p and six proteins linked to the secretory pathway: Dpm1p, Ybr159p, Yor086p, Ygr266p, and the GTPases Rho1p and Cdc42p.

Group 2 consists of 27 proteins with high P_E scores in ICAT II (>0.65) but low P_E scores (<0.6) in ICAT I. The lower ICAT I scores of Group 2 proteins reflect their primary localizations to other compartments, notably mitochondria. Indeed, 23 of these proteins are annotated in SGD as mitochon-

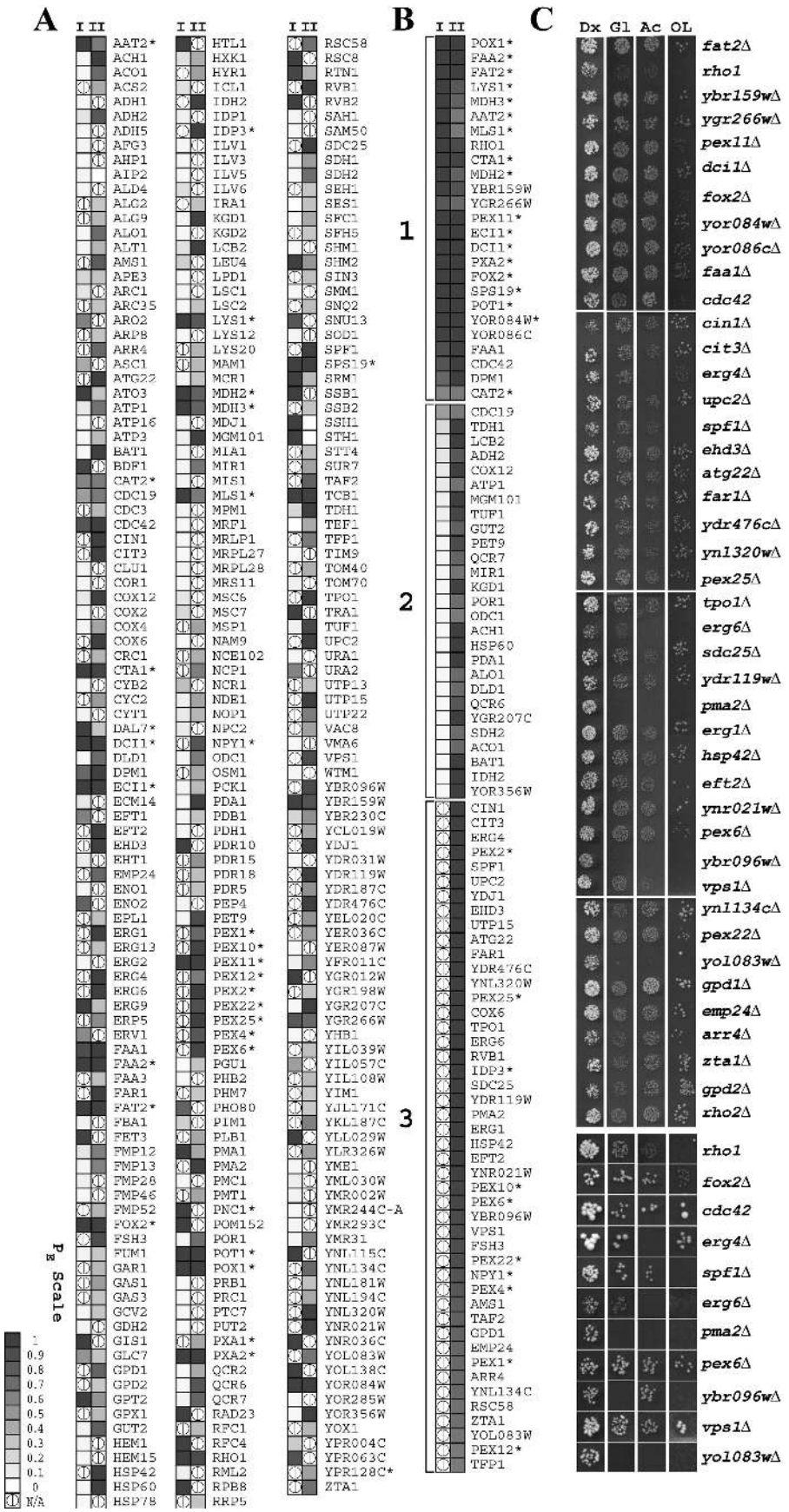

Figure 2. **Prioritization of candidates.** (A) 306 candidate proteins identified by ICAT MS/MS are listed alphabetically, and their peroxisome enrichment scores (P_E) for ICAT I or ICAT II are represented by shaded squares. See Tables S1 and S2 for details. (B) 52 candidates with P_E values > 0.65 in ICAT II, and which were also quantified in ICAT I, were clustered with a Spearman similarity metric into two groups (Groups 1 and 2). Also listed are 46 candidates with high P_E values quantified in ICAT II alone (Group 3). Known peroxisomal proteins are indicated with an asterisk. (C) Yeast mutants of selected candidates from Groups 1 and 3 were assayed for their ability to grow on rich medium (YPB) containing glucose (Dx) or an oleic acid/lauric acid mixture (OL), and, as controls, the nonfermentable carbon sources glycerol (Gl) and acetate (Ac) at 25°C. Growth was assayed 2 d (Dx), 4 d (Gl and Ac), and 7 d (OL) after spotting. Slowly growing strains (bottom panel) were also examined after 3 d (Dx), 8 d (Gl and Ac), or 20 d (OL) of growth at 25°C.

drial ($p = 6.07 \times 10^{-20}$), whereas none is annotated as peroxisomal. Based on these findings, it is unlikely that proteins in Group 2 are peroxisomal.

Proteins of Group 3 were predicted to be peroxisomal by ICAT II ($P_E > 0.65$) and were either not identified or not quantified by ICAT I. Group 3 contains 46 proteins, 10 of which have been annotated as peroxisomal ($p = 1.36 \times 10^{-12}$). Group 3 also contains seven peroxins and an uncharacterized, likely peroxin of *S. cerevisiae* identified by its homology to *Pichia pastoris* Pex22p. Notably, this group also contains Vps1p, a dynamin-related protein originally named based on its requirement in vacuolar protein sorting, but which has also been implicated in peroxisome fission (Hoepfner et al., 2001). Vps1p is predominantly cytosolic, with only a minor fraction apparently associating with peroxisomes. Together, these groups contain 31 proteins known to function in peroxisome biology, and Groups 1 and 3 make up a shortlist of proteins ($n = 71$) with the highest likelihood of having bona fide associations with peroxisomes.

As a first assessment of the potential contributions of these proteins to peroxisome function, candidate proteins in Groups 1 and 3 were assayed for their requirement in peroxisomal β-oxidation (Fig. 2 C). Strains carrying a deletion or mutation of a gene of interest were investigated for their ability to grow on medium containing a fatty acid carbon source, the metabolism of which requires functional peroxisomes. As expected, strains lacking peroxisomal β-oxidation enzymes or peroxins failed to grow, or grew slowly, on medium containing fatty acids. This was also true for the strains *vps1*Δ and *spf1*Δ (deleted for a gene encoding a putative Ca^{2+}-transporting ATPase), as well as for two strains containing temperature-sensitive alleles of *RHO1* and *CDC42*.

Candidate proteins associate with peroxisomes

Although the growth assay can serve to implicate proteins in peroxisome function, genetic redundancy, buffering, or subtle effects can allow cells lacking bona fide peroxins to still grow on oleic acid medium (for review see Hiltunen et al., 2003). Similarly, mutations in nonperoxisomal proteins could also lead to growth defects in oleic acid medium through pleiotropic or nonspecific effects. Thus, further validation of the data set came from additional localization studies of several high-scoring candidates from Groups 1 and 3. As mentioned above, the quantitative MS approach was designed to identify peroxisomal proteins but was also expected to identify proteins that might be localized to one or more additional compartments. Therefore, proteins representative of different cellular compartments were targeted: glycerol-3-phosphate dehydrogenase, Gpd1p (cytosol); a P-type ATPase, Spf1p; a protein with 3-ketoreductase activity, Ybr159p; and a COP II coat component, Emp24p (ER); the fatty acid transporter, Faa1p; the squalene epoxidase, Erg1p; and sterol 24-C-methyltransferase, Erg6p (lipid bodies); the small GTPase, Rho1p (plasma [and endo] membranes). Yeast strains containing genomically integrated protein A fusions of each candidate were made, and the behavior of each in subcellular fractionation was assessed by Western blot analysis (Fig. 3). Although each candidate was detected in fractions of low density, a portion of each also cofractionated with peroxisomes, which were detected using the peroxisomal marker proteins Fox2p, Mls1p, and Pex13p (for review see Hiltunen et al., 2003). As controls, marker proteins for endosomes and the late Golgi (Vps15p; Herman et al., 1991), the mitochondrion (Sdh2p; Robinson and Lemire, 1996), and the nucleus (Gsp1p; Moore, 1998; unpublished data) were also investigated. These proteins were not detected in the peroxisomal fractions. These data support previous studies localizing several of these components to other membranes, but also support our MS data and suggest that a subpopulation of each protein is associated with peroxisomes isolated from oleate-induced cells.

To assess further the subcellular distribution of these candidates, each candidate was tagged at its COOH terminus with GFP by genomic integration and examined by double labeling confocal microscopy to determine its localization relative to a fluorescent peroxisomal marker, peroxisomal thiolase

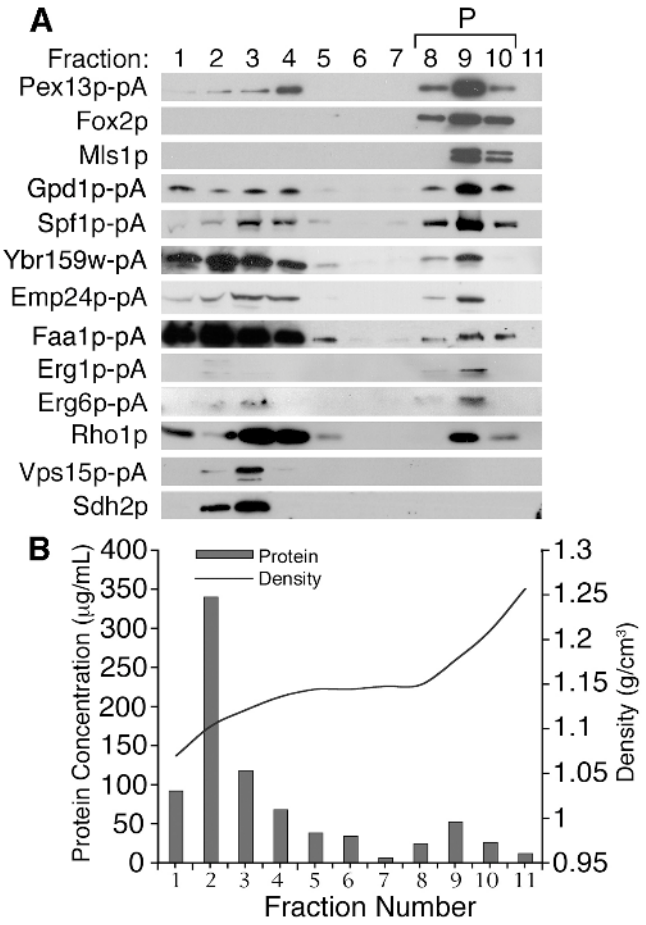

Figure 3. **Rho1p enriches with peroxisomes.** (A) Organellar 20KgP fractions from cells expressing different pA chimeras or wild-type cells were separated by isopycnic density gradient centrifugation and analyzed by Western blotting. Fractions enriched for peroxisomes (P; 8–10) were identified by the peroxisomal proteins Pex13p-pA, Fox2p, and Mls1p. Peak mitochondrial and Golgi fractions were identified by Sdh2p and Vps15p-pA, respectively. (B) The protein concentration and density profiles for each gradient fraction are presented.

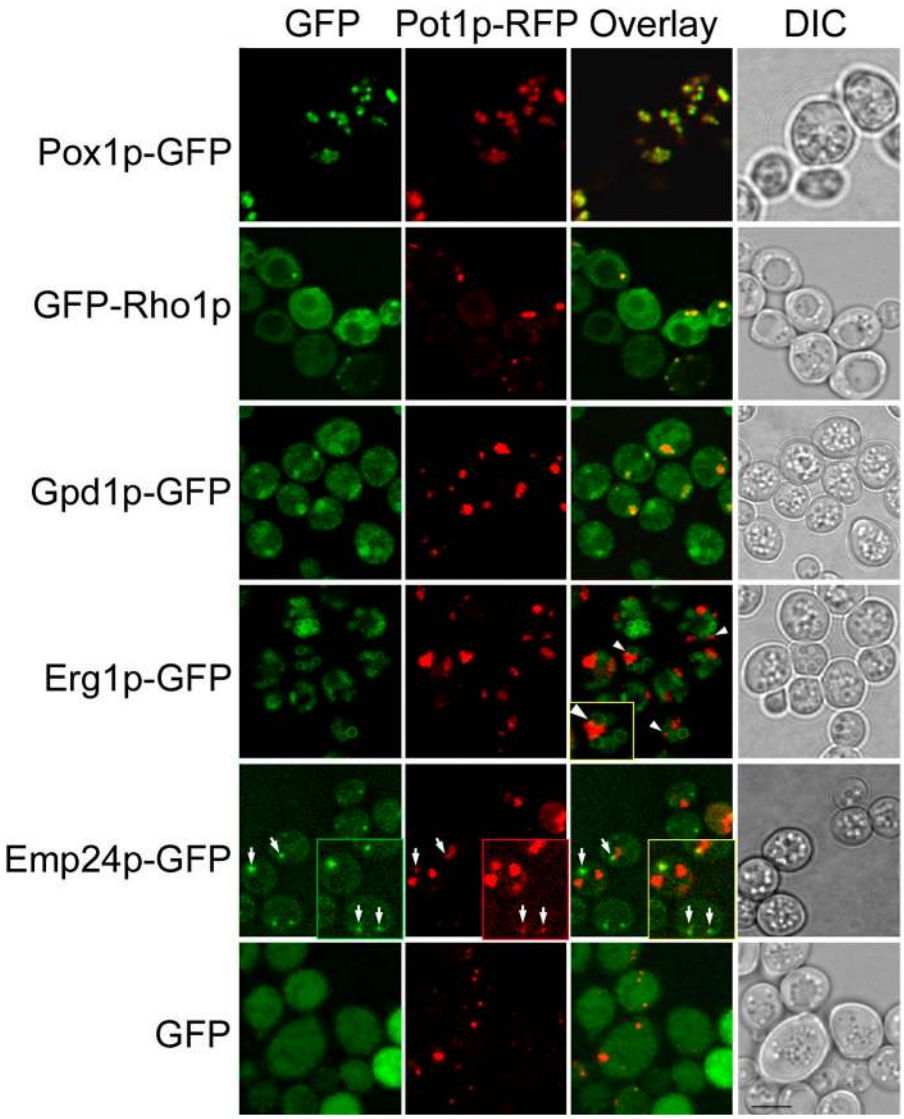

Figure 4. **Rho1p, Gpd1p, and Emp24p localize to peroxisomes.** Double labeling fluorescence confocal microscopy of yeast cells synthesizing the indicated GFP fusions and containing a plasmid coding for peroxisomal thiolase tagged with RFP (Pot1p-RFP). The GFP chimera of Pox1p (acyl-CoA oxidase) is shown as a control. GFP chimeras of Rho1p and Gpd1p showed punctate signals colocalizing with peroxisomes. The Erg1p-GFP chimera revealed a close association between peroxisomes and lipid bodies (arrowheads; inset is a higher magnification). Emp24p-GFP colocalized with small, Pot1p-RFP–labeled peroxisomes (arrows; insets are higher magnification and longer exposure). Bar, 10 μm.

(Pot1p) tagged at its COOH terminus with monomeric DsRed (RFP; Pot1p-RFP). Although we were unable to detect Spf1p-GFP or Ybr159p-GFP chimeras, the other candidates revealed distributions consistent with their subcellular fractionation behavior; each was present in nonperoxisomal structures but also colocalized with peroxisomes (Fig. 4). This was most evident for Gpd1p, the punctate signal of which colocalized exclusively with the peroxisomal marker Pot1p-RFP. Gpd1p is considered primarily as a cytosolic protein that functions to shuttle electrons from cytosolically generated NADH to the mitochondrial electron transport chain through the glycerol phosphate shuttle, regenerating NAD^+ in the process (Larsson et al., 1993). Its localization to peroxisomes raises the possibility that Gpd1p plays a similar role in peroxisomes, recycling NADH produced during peroxisomal β-oxidation of fatty acids (Hiltunen et al., 2003).

Emp24p is a COP II vesicle coat protein (Elrod-Erickson and Kaiser, 1996) and was localized primarily to punctate structures, which we interpret as ER-derived vesicles destined for the Golgi apparatus. However, close examination revealed that the Emp24p-GFP signal often overlapped with peroxisomes. These peroxisomes were generally small and of low Pot1p-RFP fluorescence intensity, suggesting they are relatively immature. This finding raises the possibility of a role for COP II vesicles in peroxisome biogenesis or maintenance. Involvement of the ER and the secretory pathway in peroxisome biogenesis remains hotly debated (Titorenko and Rachubinski, 2001; Tabak et al., 2003), and the report of interactions between Pex11p and COP I vesicles and ADP-ribosylation factor has leant support to a role for the ER and, in particular, coatamers in peroxisome budding and fission (Passreiter et al., 1998; Anton et al., 2000). However, inhibitor studies in human cells refute evidence for a significant role for COP I or COP II vesicles in peroxisome biogenesis (South et al., 2000; Voorn-Brouwer et al., 2001). Similarly, mutations in *EMP24* did not dramatically affect the biogenesis of peroxisomes in *S. cerevisiae* (unpublished data), indicating that if peroxisomes bud from the ER, Emp24p does not play an essential role in the process.

Erg1p-GFP was localized primarily to cytosolic ringlike structures characteristic of lipid particles, which are abundant in cells incubated in fatty acid medium. This same pattern was

observed with Faa1p-GFP and Erg6p-GFP (unpublished data). Interestingly, lipid bodies have been structurally and functionally associated with peroxisomes in plants (Chapman and Trelease, 1991), adipocytes (Blanchette-Mackie et al., 1995), and the yeast *Yarrowia lipolytica* (Bascom et al., 2003) and are proposed to play a role in providing lipids for the peroxisomal membrane. Here, we observed a similar association of lipid bodies with peroxisomes, extending the observations from other organisms to *S. cerevisiae*.

Rho1p is peroxisomal

Rho1p was also localized in vivo using a GFP chimera. Members of the Rho family are small, ras-related GTPases that bind to membranes via a COOH-terminal lipid modification. They act as molecular switches, cycling between the GTP- and GDP-bound states, transducing signals to stimulate actin reorganization, cell polarity, cell wall biosynthesis (in yeast), and membrane traffic (for reviews see van Aelst and D'Souza-Schorey, 1997; Hall, 1998). To preserve its normal COOH-terminal lipid modification, Rho1p was tagged as an NH_2-terminal GFP fusion. Remarkably, like the signal from Gpd1p, the punctate pattern of GFP-Rho1p matched exactly that of peroxisomes of oleic acid–incubated cells. Considering the extensive literature on Rho proteins, the localization of GFP-Rho1p to peroxisomes was particularly surprising. Moreover, Rho1p was the highest ranking novel candidate in our MS analysis, and mutants of *RHO1* had a growth defect that was significantly more pronounced on oleic acid medium (Fig. 2 C). This defect has been confirmed to be allelic to *rho1* (unpublished data). Therefore, we focused attention on Rho1p to rigorously examine its localization and used Rho1p as a means to gain new mechanistic insight into the cell biology of peroxisome biogenesis and function.

We considered the possibility that the reason Rho1p had previously not been found to be associated with peroxisomes was that yeast cells are generally grown in glucose medium, which is a condition that represses peroxisome biogenesis (Veenhuis et al., 1987). Therefore, we visualized GFP-Rho1p under conditions that repress (glucose), derepress (glycerol), or proliferate (oleic acid) peroxisomes (Fig. 5 A). Although the GFP-Rho1p signal was diffuse under all growth conditions, in glycerol and glucose the signal appeared most intense at the cell periphery and on internal membranes mainly surrounding the vacuole. This localization is consistent with current knowledge, as Rho1p has been previously localized to the plasma and endomembranes, particularly at sites of growth (for reviews see van Aelst and D'Souza-Schorey, 1997; Hall, 1998; Madden and Snyder, 1998) and has recently been shown to be required for vacuole membrane fusion (Eitzen et al., 2001). Strikingly, when cells were incubated in oleic acid medium, distinct punctate structures dominated the fluorescence signal, suggesting that Rho1p was recruited to peroxisomes upon their induction. Several mutants that affect the abundance of peroxisomes supported this interpretation, as fewer of these punctate structures were observed in *vps1*Δ cells (Fig. 5 B), which contain fewer and larger peroxisomes than wild-type cells (Hoepfner et al., 2001), and no punctate structures were observed in *pex3*Δ cells, which lack detectable peroxisomes.

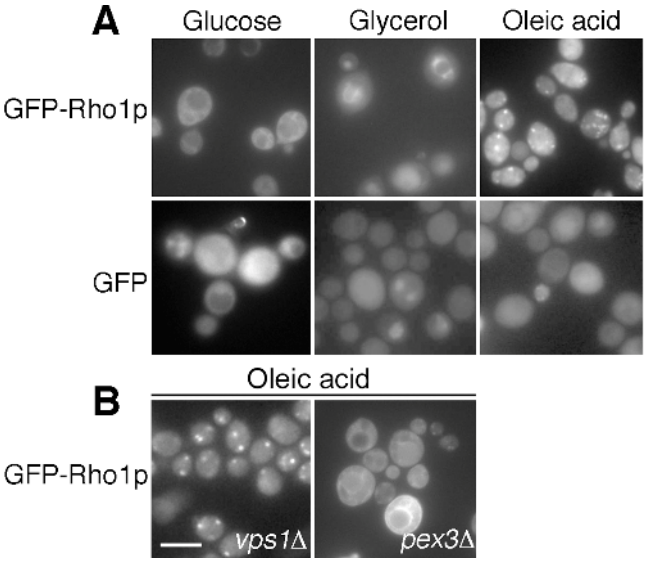

Figure 5. **Rho1p associates dynamically with peroxisomes.** The distribution of GFP-Rho1p was observed in glucose-, glycerol-, and oleic acid–incubated cells. GFP-Rho1p localized to intracellular membrane structures in glucose- and glycerol-incubated cells. In conditions that induce peroxisomes (oleic acid), GFP-Rho1p localized to distinct punctate structures. (B) In oleic acid–induced *vps1*Δ cells, which contain few peroxisomes, GFP-Rho1p localized to one or two punctate structures per cell. However, in *pex3*Δ cells, which are defective in peroxisome biogenesis, GFP-Rho1p failed to accumulate in punctate structures. Bar, 10 μm.

Together, these data highlight the dynamic association of Rho1p with peroxisomes upon their induction. These findings explain, at least partially, why fluorescence-based observations of cells in which peroxisomes were not specifically induced have previously failed to demonstrate the localization of Rho1p to peroxisomes. Moreover, MS-based proteomics efforts have also not reported an association of these other candidate proteins with peroxisomes. Our ability to detect them in peroxisome fractions is likely attributable to the ability of ICAT-based MS to identify proteins of low abundance in complex protein mixtures and the inclusion of proteins that are part of other cellular structures in the data used for analysis.

rho1 cells exhibit peroxisome defects

To investigate a role for Rho1p in peroxisome function, we first examined the peroxisome phenotypes and morphological characteristics of mutants of Rho1p. Thus, fluorescently labeled peroxisomes, detected by Pot1p-GFP, were monitored in mutant cells. Cells were incubated at permissive and semi-permissive temperatures on fatty acid medium, and peroxisome size and abundance were analyzed by confocal microscopy. At the permissive temperature of 23°C, peroxisome morphology in *rho1-2A* cells was similar to that observed in *RHO1-2A* cells (unpublished data). However, at the semi-permissive temperature of 27°C, peroxisomes in *rho1-2A* cells were smaller than peroxisomes in *RHO1-2A* cells (Fig. 6 A). In addition, *rho1-2A* cells appeared to have fewer peroxisomes than *RHO1-2A* cells, but these counts were restricted by the ability to detect peroxisomes by fluorescence microscopy. Therefore, peroxisomes that fell below the limit

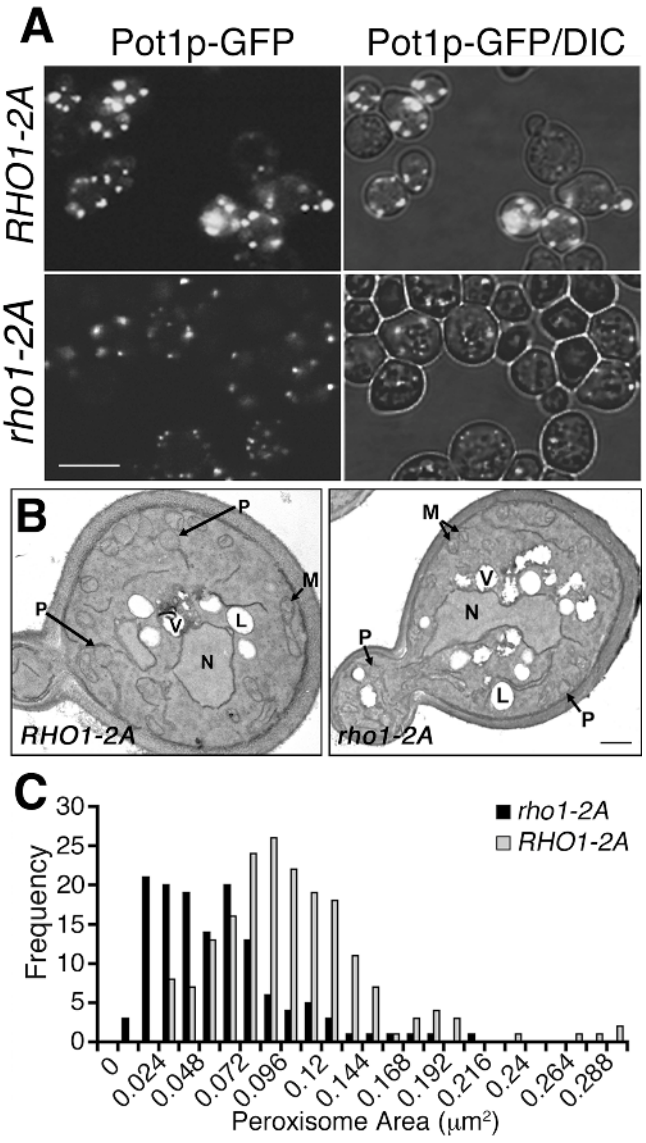

Figure 6. ***rho1* cells have fewer and smaller peroxisomes.** (A) *RHO1-2A* and *rho1-2A* cells synthesizing Pot1p-GFP were incubated in oleic acid medium for 16 h at the semi-permissive temperature of 27°C and analyzed by confocal microscopy. Bar, 10 μm. (B) *rho1-2A* and *RHO1-2A* cells were incubated in oleic acid medium at the permissive temperature of 23°C and processed for EM. N, nucleus; L, lipid body; P, peroxisome; V, vacuole; M, mitochondrion. Bar, 0.5 μm. (C) A histogram of the areas of peroxisomes calculated for 105 randomly chosen cell images of each strain is shown.

of resolution or contained small amounts of Pot1p-GFP were not quantified.

These changes in peroxisome morphology were confirmed by thin section transmission EM (Fig. 6 B). Analysis of 105 cells from each of *rho1-2A* and *RHO1-2A* strains revealed that these strains contained distinct peroxisome population distributions with respect to both size and number (Fig. 6 C). *rho1-2A* cells contained 134 peroxisomes with an average area of 0.070 ± 0.03 μm^2. In comparison, the same number of *RHO1-2A* cells contained 188 peroxisomes, and these were significantly larger (97.5% confidence level, two-sample *t* test) with an average area of 0.103 ± 0.05 μm^2.

Remarkably, when we examined the distribution of marker proteins in the *rho1-2A* strain, it appeared that peroxisomes contained a different complement of proteins than peroxisomes of wild-type cells. Wild-type and *rho1* cells were incubated at 27°C in fatty acid–containing medium, and subcellular fractions were prepared by differential centrifugation (Smith et al., 2002). As expected, Western blot analysis showed that the peroxisomal proteins Fox2p, Mls1p, Cta1p, Mdh3p, and Pot1p localized primarily to the peroxisome-enriched 20KgP fraction of wild-type cells; however, only Cta1p and Mdh3p localized to the 20KgP fraction of *rho1* cells, whereas Fox2p, Mls1p, and Pot1p were not efficiently pelleted to the 20KgP containing "normal" high-density peroxisomes (Fig. 7 A). These data suggest that *rho1* mutants were unable to incorporate all peroxisomal proteins with normal efficiency into high-density peroxisomes. Although it appeared that some proteins, such as Fox2p, were degraded due to their mislocalization, the peroxisomal proteins that remained in the 20KgS could be pelleted at higher *g*-force (200,000 *g*; unpublished data), suggesting that at least some of the mislocalized proteins were present in smaller, lighter membrane-bound compartments.

To investigate further this heterogeneity, peroxisomal protein content was monitored in vivo in *rho1-2A* and *RHO1-2A* cells synthesizing two peroxisomal reporter constructs, Pot1p-GFP and *Discosoma sp.* red fluorescent protein (DsRed)–peroxisomal targeting signal (PTS) 1 (DsRed tagged at its COOH terminus with the PTS1). Cells were incubated in oleic acid medium at 27°C, and the locations of Pot1p-GFP– and DsRed-PTS1–containing peroxisomes were analyzed by confocal microscopy (Fig. 7 B). *RHO1-2A* cells exhibited large peroxisomes that contained both Pot1p-GFP and DsRed-PTS1, as shown by the yellow color obtained by merging the signals of the individual marker proteins. In contrast, although most peroxisomes in *rho1-2A* cells contained both Pot1p-GFP and DsRed-PTS1, there were several instances in which individual peroxisomes were identified that contained either Pot1p-GFP or DsRed-PTS1, but not both (Fig. 7 B, arrowheads). Most of these occurrences were in small peroxisomes. These heterotypic peroxisomes were rarely seen in cells containing a wild-type copy of *RHO1* (*RHO1-2A*). To quantify these observations, the position and content of peroxisomes were tracked through eight 2-μm serial sections of both *rho1-2A* and *RHO1-2A* cells. 44 *rho1-2A* cells were examined and shown to contain 271 peroxisomes, of which 21 (7.7% of the total population) were characterized as being heterotypic and containing either Pot1p-GFP or DsRed-PTS1. In contrast, only 3 of the 196 peroxisomes (1.5% of peroxisomes observed in 19 cells) were labeled with only one reporter in *RHO1-2A* cells. Interestingly, few heterotypic peroxisomes were observed in *rho1-2A* cells incubated in oleic acid medium at the permissive temperature of 23°C. In cases where signals were not detected with one marker, it is possible that low protein levels hampered fluorescence detection. But there were several instances of adjacent peroxisomes in which one fluoresced brightly with one reporter and not the other, indicating that both markers were present in the same cell and the contents of the peroxisomes were different. Thus, only cells that fluoresced intensely with both mark-

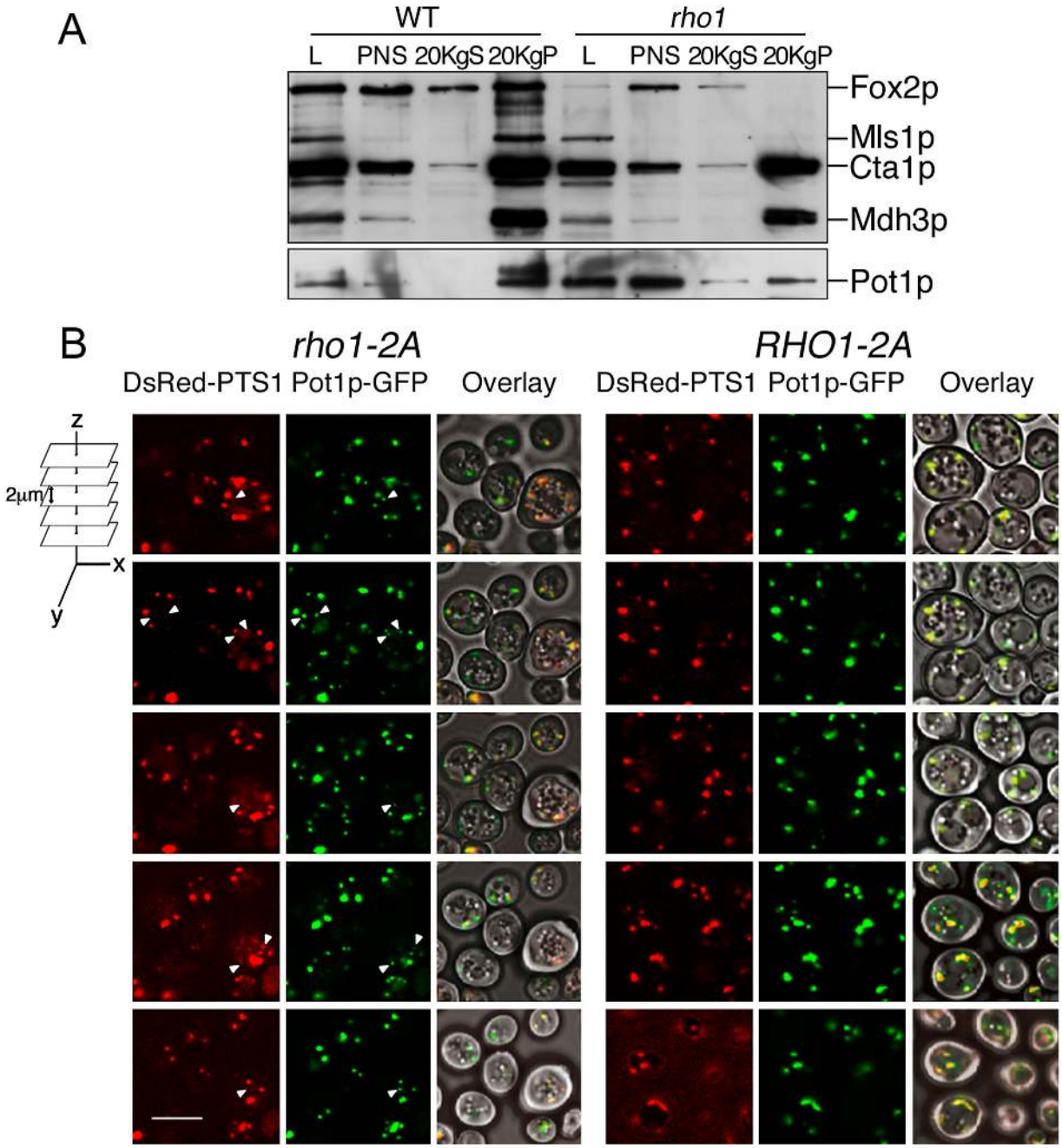

Figure 7. ***rho1* cells contain heterotypic peroxisomes.** (A) The distribution of peroxisomal enzymes in wild-type and *rho1* mutant cells was analyzed by subcellular fractionation. Whole cell lysates (L), postnuclear supernatants (PNS), and 20KgS fractions enriched for cytosol (loaded at one cell equivalent) and 20KgP fractions enriched for peroxisomes and mitochondria (loaded at five cell equivalents) were analyzed by Western blotting using anti-SKL antibodies, which recognizes PTS-1 containing proteins Fox2p, Mls1p, Cta1p, and Mdh3p, and anti-Pot1p antibodies. In *rho1* cells, the PTS1-containing proteins Fox2p and Mls1p were not detected in the 20KgP fraction, whereas PTS2-containing Pot1p was partially mislocalized to the 20KgS. (B) *rho1-2A* and *RHO1-2A* cells synthesizing the peroxisomal reporters DsRed-PTS1 and Pot1p-GFP were incubated in oleic acid medium at 27°C. A series of optical sections were obtained by confocal microscopy, and the positions of peroxisomes were determined from the signals of the Pot1p-GFP and DsRed-PTS1 reporters. Heterotypic peroxisomes containing Pot1p-GFP or DsRed-PTS1 were numerous in *rho-2A* cells (arrowheads) but were rarely observed in cells of the complemented strain, *RHO1-2A*. Bar, 10 μm.

ers were scored. Because large peroxisomes contain both reporters and likely represent mature peroxisomes, it is conceivable that small heterogeneous peroxisomes containing different complements of matrix enzymes represent immature peroxisomal precursors. These putative precursors were more readily observed in *rho1-2A* cells, suggesting a delay in the maturation of peroxisomes and, furthermore, that Rho1p has an important role in this maturation. It should be noted that the Pot1p-GFP punctate structures in *rho1* mutants could also arise from an aggregation of mislocalized Pot1p-GFP, or alternatively from its association with nonperoxisomal structures. However, aggregates were not detected in EM studies of *rho1*

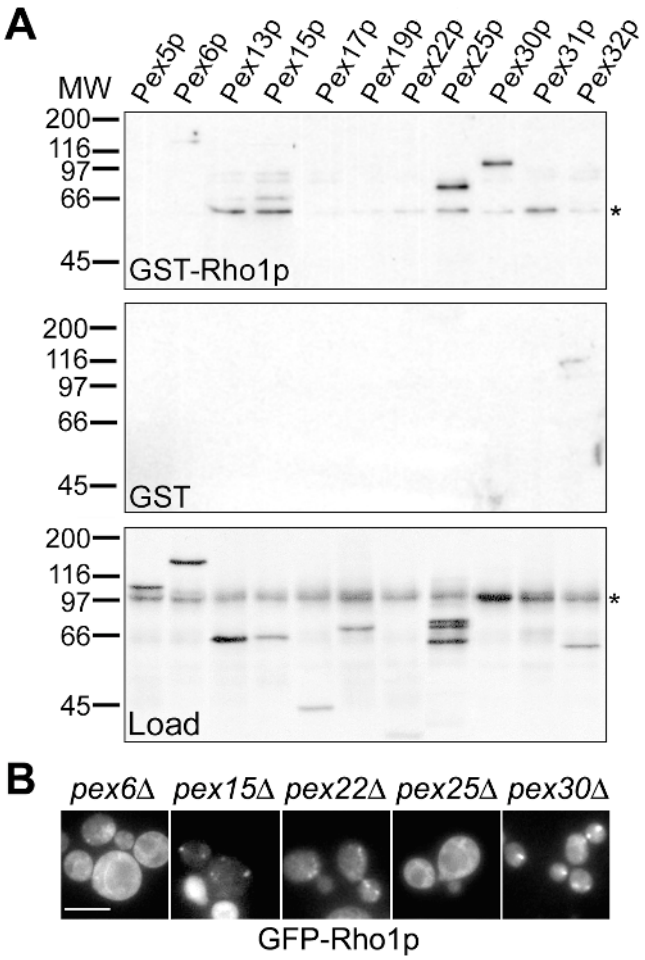

Figure 8. **Rho1p binds Pex25p and Pex30p.** GST-Rho1p and GST were immobilized on glutathione Sepharose and incubated with whole cell lysates derived from strains expressing TAP-tagged peroxins. Whole cell lysates (bottom) and bound fractions (top and middle) were resolved by SDS-PAGE, and TAP chimeras were detected by Western blotting. (top) Proteins bound to GST-Rho1p. Note that Rho1p interacts strongly with Pex25p and Pex30p. (middle) No interactions were detected with GST alone. (bottom) Yeast lysates showing the migration of each chimera. Cross-reacting bands are indicated (asterisks). (B) The distribution of GFP-Rho1p was observed in oleic acid-induced *pex6*Δ, *pex15*Δ, *pex22*Δ, *pex25*Δ, and *pex30*Δ cells. Note that GFP-Rho1p is not localized to peroxisomes in *pex25*Δ or *pex6*Δ cells. Bar, 10 μm.

mutants, nor were they observed by fluorescence microscopy in mutants (e.g., *pex7*Δ; unpublished data) in which Pot1p-GFP was mislocalized. Nevertheless, further characterization is required to determine the nature of these structures.

Rho1p and peroxisome biogenesis

To investigate the role of Rho1p on the peroxisome membrane, we sought physical interaction data between Rho1p and known peroxins. *Escherichia coli*–produced GST-Rho1p or GST alone was immobilized on glutathione resin, and yeast extracts containing TAP-tagged peroxins (Pex2p, 3p, 4p, 5p, 6p, 7p, 8p, 11p, 12p, 13p, 15p, 17p, 19p, 22p, 25p, 27p, 29p, 30p, 31p, and 32p) were incubated with the resin. Bound fractions were analyzed by Western blotting to detect the protein A chimeras. Strong interactions were observed between GST-Rho1p and Pex25p and Pex30p (Fig. 8 A). Pex25p is a cytosolically exposed peripheral peroxisomal membrane protein that appears to play a role with Pex11p and Pex27p in the regulation of peroxisome number and size, perhaps by controlling peroxisome membrane fission (or fusion; Rottensteiner et al., 2003; Tam et al., 2003). Pex30p forms a complex with Pex31p and Pex32p, and this family of integral membrane proteins also plays a role in regulating peroxisome size and number (Vizeacoumar et al., 2003).

To investigate these interactions further, Rho1p was localized in cells lacking Pex30p or Pex25p (Fig. 8 B). Importantly, these cells contain functional peroxisomes, displaying only moderate peroxisome morphological defects. Interestingly, Rho1p failed to localize to peroxisomes in cells lacking Pex25p. In comparison, Rho1p remained peroxisomal in cells lacking Pex30p (or Pex15p or Pex22p; see the following paragraph). The strong interactions between Pex25p and Rho1p, combined with the requirement of Pex25p for Rho1p recruitment to the peroxisome, argue for the specificity and functional relevance of this interaction (Fig. 8). The fact that, in *pex30Δ* cells, Rho1p association with peroxisomes was unaffected suggests that these interactions are indirect or may be related to a postrecruitment Rho1p function.

Rho1p was also found to interact with the AAA-ATPase Pex6p and its peroxisomal docking partner, Pex15p (Birschmann et al., 2003; Fig. 8 A) and weakly with Pex13p. However, because these interactions are relatively weak and *pex6*Δ, *pex15*Δ, and *pex13*Δ cells have significantly defective peroxisomes, exhibiting wholesale matrix protein import defects and remnant peroxisomal membranes, it is difficult to interpret these data with respect to potential specific docking sites. Nonetheless, we noted that *pex6*Δ and *pex13*Δ cells (unpublished data) but not *pex15*Δ or *pex22*Δ cells, which display similar peroxisomal phenotypes, failed to localize Rho1p to peroxisomes.

Rho1p and the dynamic organization of actin on peroxisomes

As Rho1p's role in membrane dynamics is thought to be mediated through its modulation of actin organization at membranes, we investigated the state of actin and its relationship to peroxisomes. In yeast, actin is found in two forms, patches and cables. Actin patches are actin-rich structures that generally cluster near active sites of secretion, and thus, mark sites of growth, whereas cables are long bundles of actin that assemble during cell division, and together with molecular motors (myosins), regulate the transport of organelles (vacuoles, mitochondria, nuclei, and peroxisomes) from mother cell to daughter cell, ensuring the faithful inheritance of each organelle.

The positions of peroxisomes and actin patches were analyzed in wild-type and mutant cells, including *rho1* cells, containing a genomically encoded Pot1p-GFP chimera to mark peroxisomes. Cells were induced to proliferate peroxisomes, and their actin was labeled with phalloidin-RITC. The relative positions of peroxisomes and actin were determined by double label confocal microscopy (Fig. 9). In wild-type cells, peroxisomes and actin patches showed different localizations, al-

though coincident staining was occasionally observed. However, in *rho1-2A* cells, peroxisomes and actin patches exhibited virtually exclusive colocalization. Although actin has been proposed to be involved in peroxisome localization within *S. cerevisiae* (Hoepfner et al., 2001), these data provide evidence for the existence of actin patches on peroxisomes and specifically a role for Rho1p in the organization of actin on this organelle. Remarkably, actin patches were also present on peroxisomes in cells lacking Pex25p, which is required for the proper localization of Rho1p to peroxisomes (Fig. 9). As a comparison, we investigated the dependence of actin localization on Pex11p and Vps1p, which are also implicated in peroxisome division and segregation. In *pex11*Δ and *vps1*Δ cells, actin was distributed as in wild-type cells. These data, together with the physical interaction data, suggest that the docking of Rho1p to Pex25p is important for dynamic assembly and disassembly of actin on peroxisomes. Interestingly, *vps1*Δ *rho1* and *pex11*Δ *pex25*Δ double mutants also showed accumulation of actin on peroxisomes, which suggests that the majority of actin is reorganized/disassembled before organelle fission and that *PEX25* is epistatic to *PEX11*.

Discussion

The molecular definition of an organelle is complicated because cellular structures are dynamic and responsive, are often derived from each other, share components with one another, and communicate with each other and the rest of the cell. Nonetheless, quantitative subcellular enrichment criteria can be used to reveal organellar liaisons and to define bona fide constituents of subcellular structures (de Duve, 1992). This principle was combined with MS to construct a prioritized list of yeast peroxisomal candidates. Although this list is by no means complete, the characterization of a subset of proteins points to a complex interplay between peroxisomes and other cellular structures. For example, these studies suggest an association of the COP II component Emp24p with small (precursor) peroxisomes, supporting the long held but disputed contention that peroxisomes are derivatives of the secretory pathway. Similarly, as observed in other cell types, we detected lipid droplet components associated with peroxisomes. The juxtaposition of lipid droplets and peroxisomes may provide a source of fatty acids for metabolism and has been proposed to provide a source of lipids for the peroxisome membrane (Chapman and Trelease, 1991; Blanchette-Mackie et al., 1995; Bascom et al., 2003). Another high ranking candidate in the MS analysis was Atg22p. Although we were unable to detect a genomically tagged version of this protein, *atg22*Δ cells were unable to efficiently degrade peroxisomes (unpublished data), suggesting a role for the association of Atg22p with the peroxisome during pexophagy. Strikingly, Gpd1p and Rho1p were both observed to be recruited to peroxisomes upon their induction in oleic acid. It is likely that Gpd1p plays a metabolic role in peroxisome biology, perhaps by analogy to its function in the glycerol phosphate shuttle, by regenerating NAD+ from NADH produced during fatty acid β-oxidation.

The top ranking candidate protein, which had not previously been localized to peroxisomes, was the GTPase Rho1p.

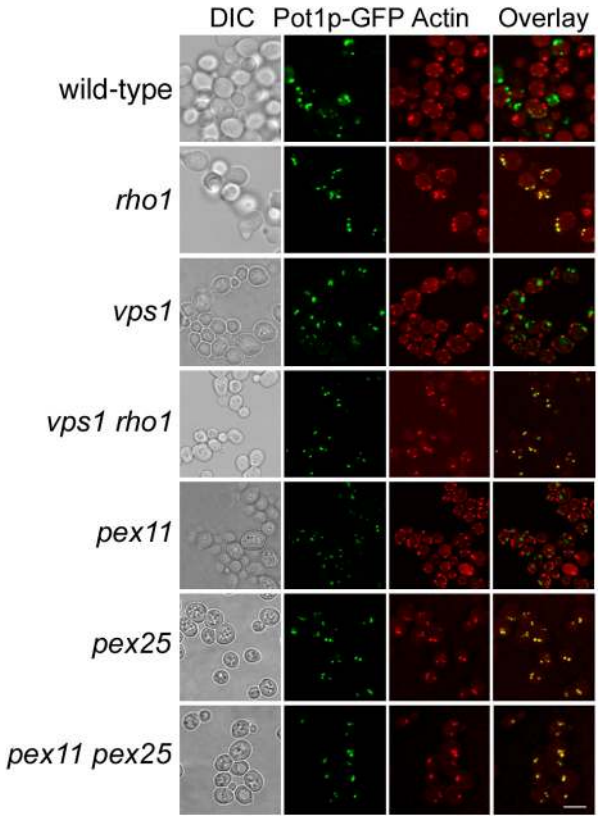

Figure 9. **Actin assembly on peroxisomes is controlled by Rho1p and Pex25p.** The subcellular distribution of actin relative to that of peroxisomes was analyzed by double fluorescence confocal microscopy. Yeast deletion mutants expressing the peroxisomal reporter Pot1p-GFP were induced in oleic acid at 30 or 23°C (for *rho1* and *vps1 rho1*) for 16 h, and actin was labeled with phalloidin-RITC. Peroxisomes colocalized with actin patches in *rho1* (*rho1-2A*) and *vps1 rho1* (*vps1*Δ *rho1 POT1-G*), *pex25* (*pex25*Δ *POT1-G*), and *pex11 pex25* (*pex11*Δ *pex25*Δ *POT1-G*) cells but not in wild-type (*POT1-G*), *vps1* (*vps1*Δ *POT1-G*), and *pex11* (*pex11*Δ *POT1-G*) cells. Bar, 10 μm.

Rho proteins have been documented to play roles in several biological processes involving the transduction of signals that result in actin reorganization and membrane dynamics (for reviews see van Aelst and D'Souza-Schorey, 1997; Hall, 1998; Madden and Snyder, 1998). Specifically, in yeast, Rho1p regulates polarized growth by organizing cortical actin patches at defined positions on the cell surface that act as targets for secretory vesicles. Fusion of vesicles to the plasma membrane results in deposition of membranes and cell wall. In addition to being implicated in exo- and endocytosis (deHart et al., 2003), Rho1p has also been shown to function in the early stages in of homotypic vacuole fusion (Eitzen et al., 2001). Unifying models of Rho1p function propose a role in the reorganization of dense membrane-associated actin patches that would otherwise provide an obstacle to membrane fusion and/or the association of membranes with molecular motor proteins, both of which are necessary to drive membrane budding and fusion (for review see Madden and Snyder, 1998).

How are actin and membrane dynamics associated with peroxisome biology? Peroxisomes are generally perceived as dynamic organelles that mature from precursor organelles that

then divide by fission. The data presented here suggest that Rho1p controls aspects of membrane dynamics important for their normal biogenesis. Considering the interaction between Rho1p and Pex25p and the apparent role of Pex25p in the late stages of peroxisome biogenesis, we propose that Rho1p-controlled actin reorganization is requisite to peroxisome fission. It is likely that actin is not completely disassembled from the peroxisome membrane during fission, but that Rho1p (and Pex25p) mediate local actin reorganization, thereby facilitating the activity of peroxins, represented by Pex11p, that control peroxisome size and number (Tam et al., 2003) and the constriction of the organelle by dynamin-like proteins such as Vps1p (Hoepfner et al., 2001).

It should be noted that membrane fission also requires localized membrane fusion, and mechanistically, membrane fusion and fission are related processes (for review see Jahn and Südhof, 1999). Considering the defined roles of Rho1p in endosomal and vacuolar vesicle fusion, the accumulation of apparently small preperoxisomal structures (Fig. 7), and the interaction between Rho1p and Pex6p (Fig. 8), which is proposed to function in peroxisomal membrane fusion (Titorenko and Rachubinski, 2000), it is possible that Rho1p also functions in peroxisome fusion during peroxisome maturation. However, it remains uncertain that peroxisomes fuse during their biogenesis, and data presented here do not speak directly to the issue of peroxisome fusion. Moreover, our analysis did not identify any peroxisomal proteins similar to the SNAREs that are involved in other membrane fusion events (for review see; Mayer, 2002). Nevertheless, the idea that preperoxisomal vesicles fuse during biogenesis is consistent with known functions for Rho1p and the accumulation of heterotypic peroxisomes in *rho1* mutant cells and similar observations in several different systems (for review see Titorenko and Rachubinski, 2001).

High throughput approaches such as the two-hybrid method, proteomics, and gene microarrays have made important contributions to biology by providing large data sets that can be mined for new biological insight. Importantly, the utility of the data sets rests on their quality and the ability to quantify the contributions of data set components to the underlying biology. With this in mind, we have combined the established principles of subcellular fractionation with modern proteomics to provide a quantitative assessment of the contribution of proteins to peroxisomal subcellular fractions. This approach is generally applicable to any subcellular fraction and has the ability to characterize known subcellular structures with greater confidence, identify new subcellular structures, and uncover new relationships between molecular compartments.

Materials and methods

Yeast strains, culture conditions, and plasmids

Yeast strains used in this study were derived from *BY4743* unless otherwise indicated (see online supplemental material). Cells were grown in medium containing 2% glucose (YEPD or YPBD), 2% glycerol (YPBG), 2% acetate (YPBA), 0.2% Tween 40, 0.15% oleic acid (YPBO or *S. cerevisiae* induction medium), or 0.15% oleic acid, 0.075 g lauric acid/L (YPBO/L), or minimal media at 30°C unless otherwise stated. Additional detail and plasmids are presented in the online supplemental material.

Microscopy

Fluorescent proteins were observed by direct fluorescence microscopy. Actin patches were stained with phalloidin-RITC and visualized by confocal microscopy. For details see the online supplemental material.

In vitro binding assay

GST and the GST-Rho1p were bound to glutathione resin and incubated with yeast cell lysates containing TAP-tagged peroxins. Bound and unbound TAP-tagged fusions were detected by Western blotting. Details are presented in the online supplemental material.

Quantitative MS

Peak peroxisome and mitochondrial fractions were isolated, and organelles were extracted to yield membrane fractions, which were differentially labeled with ICAT. For the affinity purification of peroxisomal membranes, Pex11p-pA-containing membranes were isolated by affinity chromatography using IgG-coupled magnetic beads.

Two independent experiments were performed for both ICAT I and ICAT II. In each experiment, sample pairs each consisting of 500–800 μg of protein were differentially labeled with ICAT and analyzed by μLC-ESI-MS/MS. Data were processed using SEQUEST, ASAPRatio, INTERACT, Peptide-Prophet, and Protein-Prophet. See online supplemental material.

Online supplemental material

This material includes a summary of the ICAT-MS data, the data derived from MS analysis of each protein from four ICAT experiments (Ia, Ib, IIa, and IIb) or nonquantitative gas-phase fractionation presented in Table S1, and the Gene Ontology term annotations for proteins identified by ICAT-MS presented in Table S2. Supplemental Materials and methods are also included. Online supplemental material is available at http://www.jcb.org/cgi/content/full.jcb200404119/DC1.

The authors thank H. Chan for expert assistance with EM, J. Goodman for suggesting the combination of oleic and lauric acid, B. Lemire and G. Eitzen for antibodies, S. Donohoe and K. Cooke for technical assistance, and the Institute for Systems Biology yeast group for helpful comments. We apologize to colleagues whose original research references were not cited or relegated to supplemental material due to space constraints.

J.J. Smith is a Canadian Institutes of Health Research postdoctoral fellow, Y.Y.C. Tam is an Alberta Heritage Foundation for Medical Research graduate student, and R.A. Rachubinksi is an International Research Scholar of the Howard Hughes Medical Institute and Canadian Research Chair in Cell Biology. This work was supported by National Institutes of Health grant GM067228 to J.D. Aitchison, contract N01-HV-28179 from the National Heart, Lung, and Blood Institute to R. Aebersold, and Canadian Institutes of Health Research grant MOP 53326 to R.A. Rachubinski.

Submitted: 21 April 2004
Accepted: 10 November 2004

References

Aebersold, R., and M. Mann. 2003. Mass spectrometry-based proteomics. *Nature.* 422:198–207.

Anton, M., M. Passreiter, D. Lay, T.P. Thai, K. Gorgas, and W.W. Just. 2000. ARF- and coatomer-mediated peroxisomal vesiculation. *Cell Biochem. Biophys.* 32 Spring:27–36.

Bascom, R.A., H. Chan, and R.A. Rachubinski. 2003. Peroxisome biogenesis occurs in an unsynchronized manner in close association with the endoplasmic reticulum in temperature-sensitive *Yarrowia lipolytica* Pex3p mutants. *Mol. Biol. Cell.* 14:939–957.

Baudhuin, P., H. Beaufay, and C. de Duve. 1965. Combined biochemical and morphological study of particulate fractions from rat liver. Analysis of preparations enriched in lysosomes or in particles containing urate oxidase, D-amino acid oxidase, and catalase. *J. Cell Biol.* 26:219–243.

Birschmann, I., A.K. Stroobants, M. van den Berg, A. Schafer, K. Rosenkranz, W.H. Kunau, and H.F. Tabak. 2003. Pex15p of *Saccharomyces cerevisiae* provides a molecular basis for recruitment of the AAA peroxin Pex6p to peroxisomal membranes. *Mol. Biol. Cell.* 14:2226–2236.

Blanchette-Mackie, E.J., N.K. Dwyer, T. Barber, R.A. Coxey, T. Takeda, C.M. Rondinone, J.L. Theodorakis, A.S. Greenberg, and C. Londos. 1995. Perilipin is located on the surface layer of intracellular lipid droplets in adipocytes. *J. Lipid Res.* 36:1211–1226.

Brunet, S., P. Thibault, E. Gagnon, P. Kearney, J.J. Bergeron, and M. Desjardins. 2003. Organelle proteomics: looking at less to see more. *Trends Cell Biol.* 13:629–638.

Chapman, K.D., and R.N. Trelease. 1991. Acquisition of membrane lipids by differentiating glyoxysomes: role of lipid bodies. *J. Cell Biol.* 115:995–1007.

de Duve, C. 1992. Exploring cells with a centrifuge. *In* Nobel Lectures in Physiology 1971-1980. J. Lindsten, editor. World Scientific Publishing Co., London. 152–172.

deHart, A.K., J.D. Schnell, D.A. Allen, J.Y. Tsai, and L. Hicke. 2003. Receptor internalization in yeast requires the Tor2-Rho1 signaling pathway. *Mol. Biol. Cell.* 14:4676–4684.

Eitzen, G., N. Thorngren, and W. Wickner. 2001. Rho1p and Cdc42p act after Ypt7p to regulate vacuole docking. *EMBO J.* 20:5650–5656.

Elrod-Erickson, M.J., and C.A. Kaiser. 1996. Genes that control the fidelity of endoplasmic reticulum to Golgi transport identified as suppressors of vesicle budding mutations. *Mol. Biol. Cell.* 7:1043–1058.

Gygi, S.P., B. Rist, S.A. Gerber, F. Turecek, M.H. Gelb, and R. Aebersold. 1999. Quantitative analysis of complex protein mixtures using isotope-coded affinity tags. *Nat. Biotechnol.* 17:994–999.

Hall, A. 1998. Rho GTPases and the actin cytoskeleton. *Science.* 279:509–514.

Herman, P.K., J.H. Stack, J.A. DeModena, and S.D. Emr. 1991. A novel protein kinase homolog essential for protein sorting to the yeast lysosome-like vacuole. *Cell.* 64:425–437.

Hiltunen, J.K., A.M. Mursula, H. Rottensteiner, R.K. Wierenga, A.J. Kastaniotis, and A. Gurvitz. 2003. The biochemistry of peroxisomal β-oxidation in the yeast *Saccharomyces cerevisiae*. *FEMS Microbiol. Rev.* 27:35–64.

Hoepfner, D., M. van den Berg, P. Philippsen, H.F. Tabak, and E.H. Hettema. 2001. A role for Vps1p, actin, and the Myo2p motor in peroxisome abundance and inheritance in *Saccharomyces cerevisiae*. *J. Cell Biol.* 155: 979–990.

Jahn, R., and T.C. Südhof. 1999. Membrane fusion and exocytosis. *Annu. Rev. Biochem.* 68:863–911.

Larsson, K., R. Ansell, P. Eriksson, and L. Adler. 1993. A gene encoding sn-glycerol 3-phosphate dehydrogenase (NAD+) complements an osmosensitive mutant of *Saccharomyces cerevisiae*. *Mol. Microbiol.* 10:1101–1111.

Madden, K., and M. Snyder. 1998. Cell polarity and morphogenesis in budding yeast. *Annu. Rev. Microbiol.* 52:687–744.

Mayer, A. 2002. Membrane fusion in eukaryotic cells. *Annu. Rev. Cell Dev. Biol.* 18:289–314.

Moore, M.S. 1998. Ran and nuclear transport. *J. Biol. Chem.* 273:22857–22860.

Passreiter, M., M. Anton, D. Lay, R. Frank, C. Harter, F.T. Wieland, K. Gorgas, and W.W. Just. 1998. Peroxisome biogenesis: involvement of ARF and coatomer. *J. Cell Biol.* 141:373–383.

Robinson, K.M., and B.D. Lemire. 1996. Covalent attachment of FAD to the yeast succinate dehydrogenase flavoprotein requires import into mitochondria, presequence removal, and folding. *J. Biol. Chem.* 271:4055–4060.

Rottensteiner, H., K. Stein, E. Sonnenhol, and R. Erdmann. 2003. Conserved function of Pex11p and the novel Pex25p and Pex27p in peroxisome biogenesis. *Mol. Biol. Cell.* 14:4316–4328.

Smith, J.J., M. Marelli, R.H. Christmas, F.J. Vizeacoumar, D.J. Dilworth, T. Ideker, T. Galitski, K. Dimitrov, R.A. Rachubinski, and J.D. Aitchison. 2002. Transcriptome profiling to identify genes involved in peroxisome assembly and function. *J. Cell Biol.* 158:259–271.

South, S.T., K.A. Sacksteder, X. Li, Y. Liu, and S.J. Gould. 2000. Inhibitors of COPI and COPII do not block PEX3-mediated peroxisome synthesis. *J. Cell Biol.* 149:1345–1360.

Tabak, H.F., J.L. Murk, I. Braakman, and H.J. Geuze. 2003. Peroxisomes start their life in the endoplasmic reticulum. *Traffic.* 4:512–518.

Tam, Y.Y.C., J.C. Torres-Guzman, F.J. Vizeacoumar, J.J. Smith, M. Marelli, J.D. Aitchison, and R.A. Rachubinski. 2003. Pex11-related proteins in peroxisome dynamics: a role for the novel peroxin Pex27p in controlling peroxisome size and number in *Saccharomyces cerevisiae*. *Mol. Biol. Cell.* 14:4089–4102.

Titorenko, V.I., and R.A. Rachubinski. 2000. Peroxisomal membrane fusion requires two AAA family ATPases, Pex1p and Pex6p. *J. Cell Biol.* 150: 881–886.

Titorenko, V.I., and R.A. Rachubinski. 2001. The life cycle of the peroxisome. *Nat. Rev. Mol. Cell Biol.* 2:357–368.

van Aelst, L., and C. D'Souza-Schorey. 1997. Rho GTPases and signaling networks. *Genes Dev.* 11:2295–2322.

Veenhuis, M., M. Mateblowski, W.H. Kunau, and W. Harder. 1987. Proliferation of microbodies in *Saccharomyces cerevisiae*. *Yeast.* 3:77–84.

Veenhuis, M., J.A. Kiel, and I.J. van der Klei. 2003. Peroxisome assembly in yeast. *Microsc. Res. Tech.* 61:139–150.

Vizeacoumar, F.J., J.C. Torres-Guzman, D. Bouard, J.D. Aitchison, and R.A. Rachubinski. 2003. Pex30p, Pex31p, and Pex32p form a family of peroxisomal integral membrane proteins regulating peroxisome size and number in *Saccharomyces cerevisiae*. *Mol. Biol. Cell.* 15:665–677.

Voorn-Brouwer, T., A. Kragt, H.F. Tabak, and B. Distel. 2001. Peroxisomal membrane proteins are properly targeted to peroxisomes in the absence of COPI- and COPII-mediated vesicular transport. *J. Cell Sci.* 114:2199–2204.

Weller, S., S.J. Gould, and D. Valle. 2003. Peroxisome biogenesis disorders. *Annu. Rev. Genomics Hum. Genet.* 4:165–211.

Yi, E.C., M. Marelli, H. Lee, S.O. Purvine, R. Aebersold, J.D. Aitchison, and D.R. Goodlett. 2002. Approaching complete peroxisome characterization by gas-phase fractionation. *Electrophoresis.* 23:3205–3216.